Journal of Solid State Chemistry 182 (2009) 849–854

Contents lists available at ScienceDirect

Journal of Solid State Chemistry

journal homepage: www.elsevier.com/locate/jssc

Chemical vapor deposition and electric characterization of perovskite oxides $LaMO_3$ (M = Co, Fe, Cr and Mn) thin films

Patrick Herve Tchoua Ngamou, Naoufal Bahlawane *

Department of Chemistry, Bielefeld University, Universitätsstr. 25, 33615 Bielefeld, Germany

ARTICLE INFO

Article history:
Received 18 August 2008
Received in revised form
3 December 2008
Accepted 17 December 2008
Available online 4 January 2009

Keywords:
Pulsed spray evaporation CVD
Perovskite thin films
Electrical characterization

ABSTRACT

Oxides with a perovskite structure are important functional materials often used for the development of modern devices. In view of extending their applicability, it is necessary to efficiently control their growth as thin films using technologically relevant synthesis methods. Pulsed spray evaporation CVD was used to grow several perovskite-type oxides on planar silicon substrates at temperatures ranging from 500 to 700 °C. The optimization of the process control parameters allows the attainment of the perovskite structure as a single phase. The electrical characterization using the temperature-dependent conductivity and thermopower indicates the p-type conduction of the grown films and shows a decreasing concentration of the charge carrier, mobility and band gap energy in the sequence $LaCoO_3 > LaMnO_3 > LaCrO_3 > LaFeO_3$. The investigation of the electric properties of the obtained perovskite thin films shows the versatility of CVD as a method for the development of innovative devices.

1. Introduction

Perovskite-type transition metal oxides constitute an important class of materials due to their electrical, magnetic and catalytic properties. Theses properties allow them to be used as catalysts for hydrocarbon oxidation [1–3] and the control of automobile emissions [4,5], electrode and interconnect materials for solid oxide fuel cells (SOFC) [6–8], sensor materials for reducing gases such as CO and alcohols [9–11] and as thermoelectric devices [12]. In particular $LaCrO_3$ and $LaCoO_3$ are intensively investigated as electrodes for fuel cells [13,14], $LaMnO_3$ and derived compounds exhibit colossal magnetoresistive effect that is exploited for the development of submicrometer magnetic field sensors [15] whereas $LaFeO_3$ was involved to induce ferromagnetic–antiferromagnetic exchange bias effect, exploited for the development of advanced magnetic read heads and magnetic memory cells [16]. Unlike bulk ceramics, thin films of these materials would allow the integration of their functionalities in a number of modern devices, e.g. as on-chip temperature sensors or as on-chip cooling systems [17]. In this respect, magnetron sputtering is repeatedly used as a process to grow perovskite thin films [18,19]. Much attention was given to their preparation method since their performances were noticed to strongly depend on the synthesis procedure. For instance, it has been found that the microstructure, the electric and magnetic properties of thin films are different from those reported for the corresponding bulk materials [20,21]. Although chemical vapor deposition (CVD) is particularly advantageous as a non-line-of-sight, high throughput and low-cost process, it was rarely applied for the growth of perovskite films such as $LaMO_3$ (M = Co, Mn, Cr and Fe) [22]. The limited use of CVD for the growth of perovskites is likely due to the difficulty to simultaneously control the supply of two precursors, which was solved in a two-steps strategy; hybrid CVD/sol–gel [23,24]. The performance of the CVD process depends highly on the properties of the source materials and the delivery technique. Liquid delivery of the precursor exhibits numerous advantages when compared to the conventional bubbler delivery. These advantages include the less demanding criteria in terms of precursor properties and the accurate control of the composition in the case of the deposition of mixed oxides and alloys [25,26]. This study shows the suitability of pulsed spray evaporation (PSE)-CVD to grow these materials as thin films, and reports their electric properties in comparison with the corresponding bulk materials.

2. Experimental

The growth of the $LaMO_3$ perovskite thin films was performed in a cold-wall stagnation point-flow CVD reactor, which is equipped with a pulsed spray evaporation (PSE) system for the delivery of liquid precursor feedstocks. More details about the deposition set up can be found elsewhere [26,27]. The concentration of lanthanum acetylacetonate in the feedstock was fixed at

* Corresponding author. Fax: +49 521 106 6027.
E-mail address: naoufal@pc1.uni-bielefeld.de (N. Bahlawane).

0022-4596/$ - see front matter © 2009 Elsevier Inc. All rights reserved.
doi:10.1016/j.jssc.2008.12.017

2.5 mM, while that of the transition-metal acetylacetonate precursor was adjusted between 0.5 and 2.5 mM in order to obtain stoichiometric single-phase perovskite films. Metal acetylacetonate precursors $Co(acac)_2$, $Cr(acac)_3$, $Fe(acac)_2$, $Mn(acac)_2$ and $La(acac)_3$ are purchased from STREM Chemicals and are used as received. The precursors were dissolved in ethanol, mixed with the desired ratios and kept at room temperature under atmospheric pressure during deposition. Metal acetylacetonates were selected in this study as precursors owing to their stability and high solubility in ethanol. Furthermore, most metals are commercially available as acetylacetonate complexes, which the combined use is not affected by the ligand exchange reaction. The PSE delivery was achieved with a valve opening time of 2.5 ms and a frequency of 14 Hz enabling an average feeding rate of 570 μl min^{-1}. The evaporation of the injected feedstock takes place at 220 °C in the tubular 30 cm-long evaporation chamber, where a complete evaporation of the precursors in addition to ethanol takes place. The resulting vapor was transported to the deposition chamber with N_2/O_2 flow rates of 0.1/2 slm. During the transport step, the reaction of the transition metal acetylacetonate with ethanol solvent or oxygen can not be excluded. Planar silicon substrates were heated using a flat resistive heater. The substrate temperature was chosen in the range of 500–700 °C during deposition, while the total pressure in the reactor was kept at 30 mbar. The identification of the crystalline phase of the grown films was performed using X-ray diffraction (XRD, PHILIPS X'Pert Pro MDR) under ambient conditions, and the crystallite sizes (D) were calculated by means of the Scherrer's equation from the widening of the diffraction peaks. The thickness of the obtained films was estimated gravimetrically using a microbalance (Mettler ME30, digital resolution of 1 μg), while the microstructure was examined using scanning electron microscopy (SEM, S-450 Hitachi). Conductivity measurements were performed in air atmosphere and up to 560 °C using a PC-controlled four-probe d.c. equipment. The electrical conductivity was measured starting from room temperature except for $LaFeO_3$, which was only measurable starting at a temperature of 220 °C. The thermopower was assessed using K-thermocouples to measure the applied temperature gradient and platinum electrodes to measure the resulting voltages. In order to avoid the influence of the substrate during the electrical characterization, a thin film of α-Al_2O_3 was grown by CVD starting from $AlCl_3$ precursor [28]. The α-Al_2O_3 layer provides an electrical insulation up to 900 °C in the measurement conditions of voltage and current. Therefore, the electrical and thermopower properties were measured on α-Al_2O_3 coated silicon substrates using perovskite films with a thickness of 250 nm.

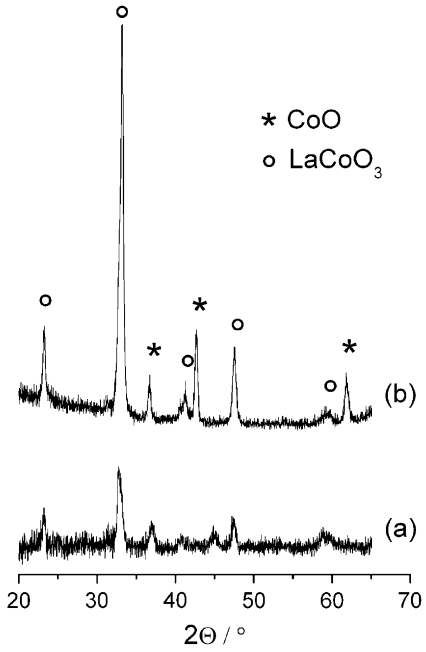

Fig. 1. XRD patterns of 130 nm-thick films deposited using $R = 1$ and a substrate temperature of (a) 600 °C and (b) 700 °C. Diffraction peak at 45° corresponds to the spinel cobalt oxide.

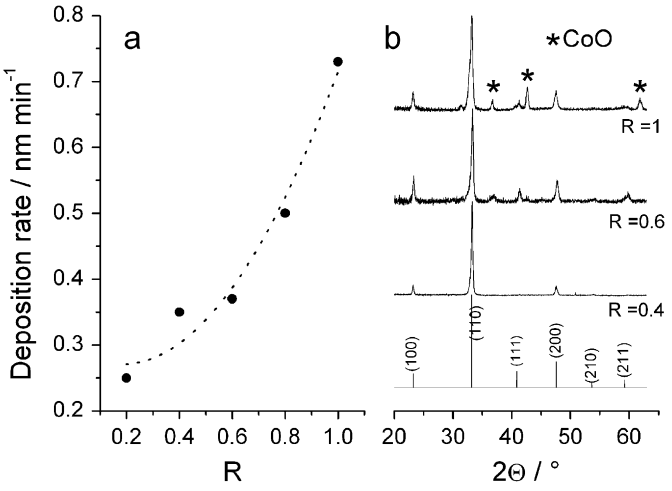

Fig. 2. Evolution of the growth rate (a) and XRD-patterns (b) as a function of R for $LaCoO_3$ films deposited at 700 °C for 3 h. The indexes correspond to the reference database of the perovskite $LaCoO_3$ (PDF Nr 75-0279/ cubic $Pm3m$).

3. Results and discussion

3.1. Growth and characterization

Before undertaking the deposition investigations of the perovskite $LaCoO_3$ films, the growth of La_2O_3 and of CoO/Co_3O_4 was performed starting from the corresponding acetylacetonate complexes. This step determines the operating window where both materials grow readily. Fig. 1 shows the XRD patterns of $LaCoO_3$ films obtained after 3 h of deposition on Si(100) at substrate temperatures of 600 and 700 °C. In this case, an equimolar concentration of the precursors was used in the feedstock ($R = 1$, R is defined as the precursors concentration ratio in the feedstock; $R = [Co(acac)_2]/[La(acac)_3] = 1$).

The diffraction peaks show the coexistence of the cubic lanthanum cobaltate (PDF-Nr 75-0279), the cubic cobalt monoxides (PDF-Nr 75-0533) and the spinel cobalt oxide Co_3O_4 (PDF-Nr 42-1467). Increasing the deposition temperature from 600 to 700 °C suppresses the formation of Co_3O_4 and leads to an increase of the intensity of the diffraction peaks of both phases, $LaCoO_3$ and CoO, indicating the improvement of the film crystallinity. The preferential incorporation of cobalt into the film, within this temperature range, indicates the larger sticking probability of $Co(acac)_2$ relative to that of $La(acac)_3$. Thus, the excess of cobalt in the film forms the CoO phase. In this investigation, it is clear that the co-formation of the cobalt monoxide phase cannot be simply suppressed by adjusting the deposition temperature. Therefore, the effect of the metals' stoichiometry in the liquid feedstock was investigated by decreasing the concentration of $Co(acac)_2$ precursor. As depicted in Fig. 2a for films grown at 700 °C, the growth rate of the films decreases generally with the decrease of R, which indicates that the growth kinetic is mainly controlled by the concentration of $Co(acac)_2$ precursor in the feedstock.

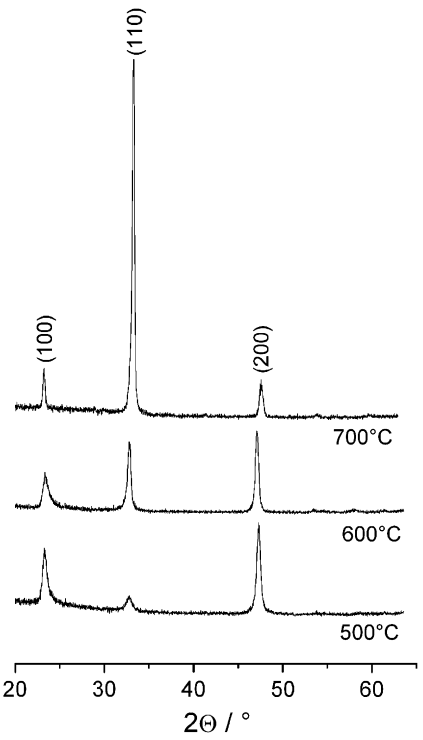

Fig. 3. XRD patterns of $LaCoO_3$ films deposited with $R = 0.4$ at substrate temperature varying from 500 to 700 °C.

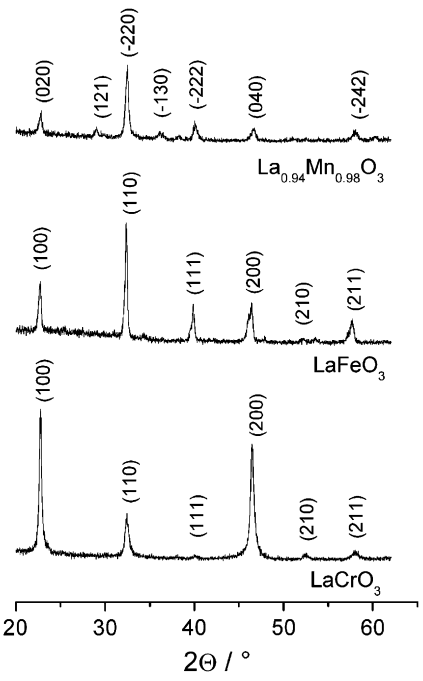

Fig. 4. XRD patterns of $LaCrO_3$, $LaMnO_3$ and $LaFeO_3$ obtained after 3 h of deposition on Si(100) substrates. The indexes correspond to the reference database of the corresponding perovskites $LaCrO_3$ (PDF Nr 75-0288/ cubic *Pm*3*m*), $La_{0.94}Mn_{0.98}O_3$ (PDF Nr 85-0372/ rhombohedral R-3c) and $LaFeO_3$ (PDF Nr 75-0541/ cubic *Pm*3*m*).

Decreasing the ratio R allows an efficient limitation of the formation of CoO, which is attained at $R = 0.4$ as illustrated in Fig. 2b, where only the cubic (*Pm*3*m*) $LaCoO_3$ (PDF-Nr 75-0279) with a (110) preferred orientation is obtained. Decreasing the deposition temperature in these conditions to 500 °C favors the (100) orientation as indicated in Fig. 3.

In this section we demonstrated the possibility to grow perovskite as a pure phase using the PSE-CVD process through the accurate adjustment of the feedstock composition. In fact, the liquid delivery in this case presents a useful tool to overcome the inherent contrast between the sticking probabilities of various precursors in the dual-source strategy for the growth of multi-component films. It is also shown that the deposition temperature remarkably influences the growth orientation of the film.

Comparable optimization procedures, as for $LaCoO_3$, were performed for other transition metals to grow $LaMnO_3$, $LaFeO_3$ and $LaCrO_3$ thin films. The XRD patterns of the grown $La_{0.94}Mn_{0.98}O_3$, $LaFeO_3$ and $LaCrO_3$ films, Fig. 4, show pure perovskite phases. $La_{0.94}Mn_{0.98}O_3$ (PDF Nr 85-0372) crystallizes in the rhombohedral R-3c lattice while $LaCrO_3$ (PDF Nr 75-0288) and $LaFeO_3$ (PDF Nr 75-0541) crystallize in the cubic (*Pm*3*m*) lattice.

As shown in Table 1, $LaMnO_3$ and $LaCrO_3$ require an equimolar feedstock ($R = 1$), while $LaCoO_3$ and $LaFeO_3$ are grown with $R = 0.4$. The delivery parameters and the deposition pressure are mentioned in the experimental part. SEM micrographs, Fig. 5, show comparable film morphology for $LaCoO_3$ and $LaFeO_3$ with compact spherical grains, whereas $LaCrO_3$ exhibits a cauliflower structure with apparent open porosity. The obtained $LaMnO_3$ film is composed of spherical particles that build closely packed film with a relatively rough surface. The cross-sectional view shows a granular texture that grows in a columnar way forming a dense film.

3.2. Electrical characterization

Fig. 6a displays the temperature-dependent electrical conductivity of La*M*O_3 films (M = Cr, Mn, Co and Fe) up to 600 °C. The

Table 1
Growth characteristics of $LaFeO_3$, $LaMnO_3$, $LaCoO_3$ and $LaCrO_3$ films.

Characteristics	$LaFeO_3$	$LaMnO_3$	$LaCoO_3$	$LaCrO_3$
Substrate temperature (°C)	700	700	700	750
$R = [M^a(acac)_n]/[La(acac)_3]$	0.4	1	0.4	1
Growth rate (nm min^{-1})	0.73	0.48	0.79	1.39
Average crystallite size (nm)	63	57	53	60

[a] M = Fe, Mn, Co and Cr.

investigated perovskites exhibit an increased conductivity with increased temperature over the measured temperature range, which is a typical semiconductor behavior [29].

At 230 °C, the electrical conductivity of $LaCoO_3$ increased dramatically compared to the other deposited films. For instance, at 430 °C, the electrical conductivity of $LaCoO_3$ is about two orders of magnitude larger than that of $LaFeO_3$ and one order of magnitude larger than that of $LaCrO_3$. This trend is in agreement with that reported in literature for bulk ceramics with the similar compositions [30–32]. The electrical conductivity of $LaFeO_3$ at 560 °C was measured to be 0.39 S cm^{-1}, which is close to the value of 0.36 S cm^{-1} for bulk $LaFeO_3$ reported by Hung et al. [33]. $LaMnO_3$ presents a conductivity of 4.80 S cm^{-1} at 560 °C, which is close to ~5.5 S cm^{-1} reported by Fujihira et al. [34] for films prepared on Al_2O_3 substrates using the sol–gel method. The electrical conductivity mechanism of La*M*O_3 (M = Cr, Co, Fe and Mn) perovskite oxides has been discussed by several authors. It is largely accepted in the literature [34–36] that the charge transfer occurs via the *M*–O–*M* bonds due to the exchange of the electronic state of the transition metal between M^{+4} and M^{+3}. It is worth noting that the transition metal (M) in La*M*O_3 perovskites is present in the M^{+3} oxidation state.

The measurement of the thermoelectric power was performed with the objective to identify the charge carriers (electron or hole)

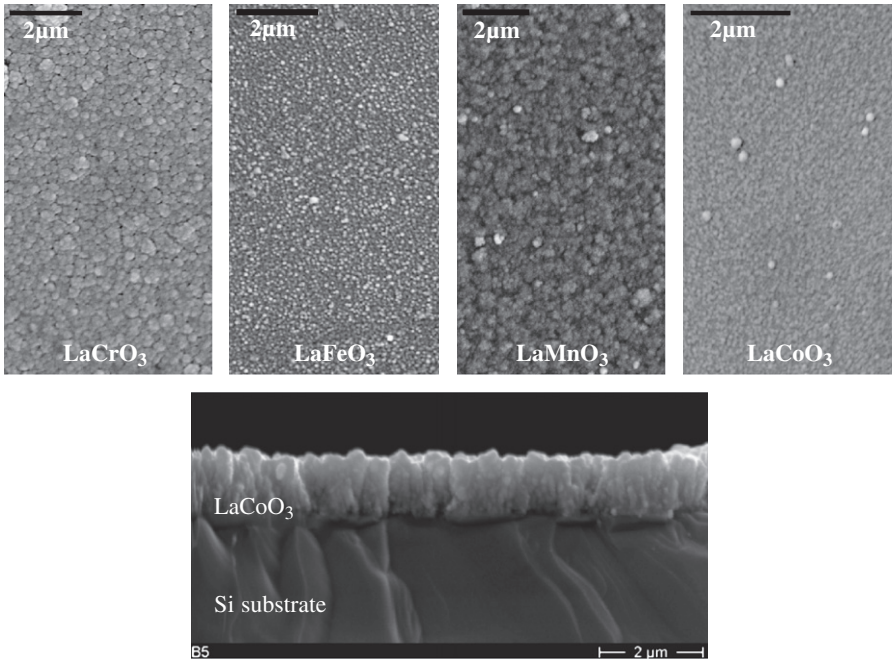

Fig. 5. SEM surface micrographs of perovskite films and a cross-section view where $LaCoO_3$ is selected as an illustrative example. (Deposition conditions are listed in Table 1.)

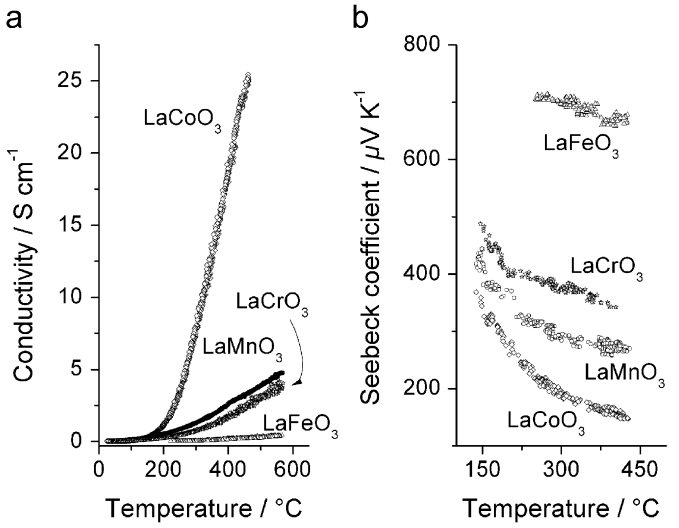

Fig. 6. Temperature dependence of the electrical conductivity (a) and Seebeck coefficient (b) of 250 nm thick LaMO_3 films (M: Cr, Mn, Fe and Co).

and to determine their concentrations as a function of the temperature. The temperature-dependent Seebeck coefficient (S), depicted in Fig. 6b, shows positive values in the entire investigated temperature range indicating a p-type conduction behavior. Therefore, the electrical conduction occurs via the mobility of the holes as noticed for the corresponding bulk materials [30,32,37,38]. The measurement of S for $LaFeO_3$ film was restricted to the temperature range where the electrical conductivity was accurately measured. In order to calculate the fraction of sites carrying the charge (C) we have used the Heikes formula (1) that links this parameter to the Seebeck coefficient [38,39]:

$$S - S_0 = \frac{k}{e} \ln\left(\frac{1-C}{C}\right), \tag{1}$$

Table 2
Electrical properties of the perovskites as measured at 430 °C, including the mobility activation (E_μ) energy and the gap energy (E_g).

Characteristic	$LaCoO_3$	$LaMnO_3$	$LaCrO_3$	$LaFeO_3$
σ (S cm^{-1})	22.29	3.08	2.03	0.201
E_μ (eV)	0.512 ± 0.002	0.281 ± 0.0006	0.32 ± 0.0005	0.33 ± 0.002
E_g (eV)	0.37 ± 0.004	0.287 ± 0.005	0.24 ± 0.006	0.20 ± 0.01
C (%)	15.6	4.6	1.9	0.03
μ (m^2/V s)	1.55×10^{-08}	1.093×10^{-09}	6.09×10^{-10}	3.99×10^{-13}

where k is the Boltzmann constant, e is the electronic charge and S_0 is generally neglected because its value is supposed to be less than 10 μV/K [38]. For illustrative purposes, the fraction of sites carrying the charge at 430 °C is given in Table 2. The gap energy (E_g) of the grown perovskites was calculated according to the formula (2) [40].

$$C = C_0 \exp\left(\frac{-E_g}{2kT}\right), \tag{2}$$

where C_0 is a temperature-independent constant. The Arrhenius plots, ln(C) versus $1/T$ derived from Eq. (2), allow the determination of the band gap energies (E_g) that are listed in Table 2. The band gaps measured here with perovskite thin films agree reasonably with the calculated fundamental band gapes by local spin-density approximation method [41,42] (LSDA) as illustrated in Table 3. Good agreement is also observed with the measured band gaps with conductivity-based methods for the corresponding bulk materials as shown in Table 3 for $LaCoO_3$ [43–46] and $LaMnO_3$ [47]. Nevertheless, except for $LaCoO_3$ [48,49] all other perovskites present band gaps that largely diverge from these measured with optical methods [48–50], which is presumably linked to the contrasting sensitivity of both methods to various transitions.

The mobility of the charge carrier (μ) was calculated from the measured conductivity (σ) and the fraction of sites carrying the

Table 3
Comparison between the measured and literature gap energy values.

	E_g (eV) (this work)	E_g (eV)	Method	Reference
$LaCrO_3$	0.24	0.6	Fundamental gap (LSDA)	Solovyev et al. [41]
		3.4	Optical method	Arima et al. [48]
$LaMnO_3$	0.287	0.2	Fundamental gap (LSDA)[a]	Solovyev et al. [41]; Sarma et al. [42]
		0.24	Electrical resistivity	Mahendiran et al. [47]
		1.1	Optical method	Arima et al. [48]
		1.7	Optical method	Saitoh et al. [50]
$LaFeO_3$	0.2	2.1	Optical method	Arima et al. [48]
		0.2	Fundamental gap (LSDA)[a]	Solovyev et al. [41]
		0.3	Fundamental gap (LSDA)[a]	Sarma et al. [42]
$LaCoO_3$	0.37	0.35	Electrical resistivity	Gerthsen and Härdtl [43]
		0.37	Electrical resistivity	Dorder et al. [44]
		0.32–1.1 $\times 10^{-4}$ T	Electrical resistivity	Jonker et al. [45]
		0.3	Optical method	Arima et al. [48]
		0.2	Electrical resistivity	Bhide et al. [46]
		0.2	Fundamental gap (LSDA)[a]	Solovyev et al. [41]; Sarma et al. [42]
		0.6	Optical method	Chainani et al. [49]

[a] Local spin-density approximation including the electron–electron interactions (LDA+U).

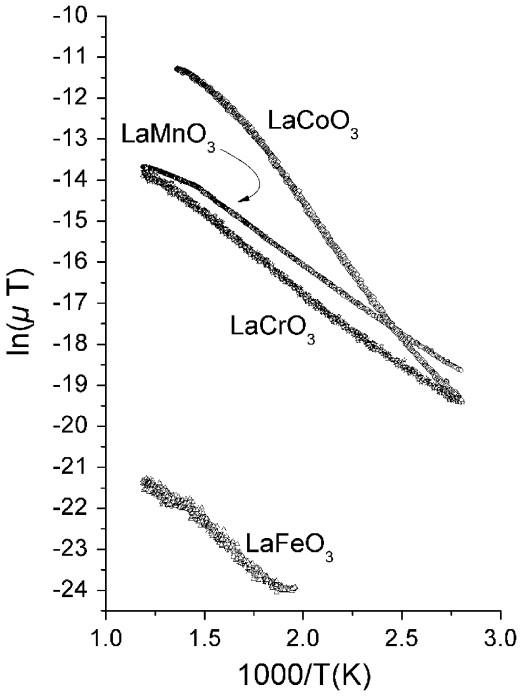

Fig. 7. Arrhenius plots $\ln(\mu T)$ versus $1/T$ of the mobility for the perovskite films.

charge (C) according to Eq. (3) [40,51]:

$$\sigma = NCe\mu \tag{3}$$

where N is the total number of sites per unit volume. The carrier mobility is expected to increase with the temperature since it is thermally activated with an energy of E_μ. For illustrative purposes, the mobility was given in Table 2 at 430 °C. The values of μ, for thin films, lie in the range of 10^{-8}–10^{-13} $m^2 V^{-1} sec^{-1}$ that overlaps with that reported for bulk materials (10^{-6}–10^{-9} $m^2 V^{-1} sec^{-1}$) [36]. The relatively lower charge mobility might be attributed to the high density of grain-boundaries due to the nano-sized particles forming the thin films. The calculated temperature-dependent charge mobility was exploited to derive the mobility activation energy of this process according to Eq. (4) [40,51]. The corresponding plot is depicted in Fig. 7:

$$\mu = \frac{A}{T}\exp\left(-\frac{E_\mu}{kT}\right). \tag{4}$$

The calculated value of the mobility activation energy for each $LaMO_3$ film is given in Table 2. $LaCoO_3$ film exhibits a mobility activation energy of 0.512 eV, which agrees with the reported value by Losurdo et al. [35] (0.55 eV) using nanostructured $LaCoO_3$ thin film that was prepared by hybrid sol–gel and CVD method.

The increase of the electrical conductivity with the temperature shows the semiconducting behavior of $LaMO_3$ films, whereas linearity between $\log(\mu T)$ and $1/T$ indicates that the mobility is thermally activated as expected for small polaron hopping. The obtained positive values of the Seebeck coefficient confirm that the dominant charge carriers are holes. Therefore, the electrical conductivity occurs by thermally activated jumps of holes from M^{4+} cation to nearby M^{3+} via the intermediate oxygen ions. It has also been reported [52] that the successive jump of the hole along the ($M^{4+} \rightarrow O^{2-} \rightarrow M^{3+}$) chain is slightly influenced by the Coulomb repulsion interaction due to the presence of La^{3+} ions. The fraction of M^{4+} sites was calculated here in agreement with the mobility and the conductivity behavior to follow the sequence $LaCoO_3 > LaMnO_3 > LaCrO_3 > LaFeO_3$. These differences in electrical conductivity and mobility should be related to the differences of band structure and energy gap of each sample. As a matter of fact, the highest hole concentration in $LaCoO_3$ implies the lowest Fermi energy close to the valence band and consequently the highest gap energy. This explanation was confirmed by calculating the band gap energy of each film from the Arrhenius plot of fractional carrier concentration.

4. Conclusion

Pure $LaMO_3$ (M = Cr, Co, Mn and Fe) perovskite films were successfully produced by PSE-CVD starting from ethanol solution of the corresponding metal acetylacetonate precursors. The principal control parameter for the deposition of single $LaMO_3$ phase was the precursor concentration ratio (R) in the feedstock. All $LaMO_3$ films exhibit p-type conduction (i.e. holes are the

dominant charge carriers). The fraction of sites carrying the holes, the band gap energy calculated from the experimentally measured Seebeck coefficients, and the carrier mobility values are consistent with the electrical conductivity measurements. These data show that PSE-CVD is a versatile method for the preparation of perovskites thin films for high temperature applications.

Acknowledgments

One of the authors (PHTN) thanks Deutscher Akademischer Austausch Dienst (DAAD) for his fellowship grant at the University of Bielefeld in Germany. Useful discussions with Katharina Kohse-Höinghaus are gratefully acknowledged.

References

[1] K.S. Song, H.X. Cui, S.D. Kim, S.K. Kang, Catal. Today 47 (1999) 155–160.
[2] M. O'Connell, A.K. Norman, C.F. Huttermann, M.A. Morris, Catal. Today 47 (1999) 123–132.
[3] R. Spinicci, M. Faticanti, P. Marini, S. De Rossi, P. Porta, J. Mol. Catal. A Chem. 197 (2003) 147–155.
[4] R. Doshi, C.B. Alcock, J.J. Carberry, Catal. Lett. 18 (1993) 337–343.
[5] R.J.H. Voorhoeve, J.P. Remeika, L.E. Trimble, A.S. Cooper, F.J. Disalvo, P.K. Gallagher, J. Solid State Chem. 14 (1975) 395–406.
[6] M.B. Phillipps, N.M. Sammes, O. Yamamoto, J. Mater. Sci. 31 (1996) 1689–1692.
[7] S.P. Jiang, L. Liu, P.O.B. Khuong, W.B. Ping, H. Li, H. Pu, J. Power Sources 176 (2008) 82–89.
[8] X.F. Ding, Y.J. Liu, L. Gao, L.C. Guo, J. Alloy. Compds. 425 (2006) 318–322.
[9] D.T. Anh, W. Olthuis, P. Bergveld, Sensors Actuators B Chem. 103 (2004) 165–168.
[10] X. Liu, B. Cheng, J.F. Hu, H.W. Qin, M.H. Jiang, Sensors Actuators B Chem. 129 (2008) 53–58.
[11] L.B. Kong, Y.S. Shen, Sensors Actuators B Chem. 30 (1996) 217–221.
[12] A. Weidenkaff, R. Robert, M. Aguirre, L. Bocher, T. Lippert, S. Canulescu, Renewable Energy 33 (2008) 342–347.
[13] J. Sfeir, P.A. Buffat, P. Mockli, N. Xanthopoulos, R. Vasquez, H.J. Mathieu, J. Van herle, K.R. Thampi, J. Catal. 202 (2001) 229–244.
[14] S.J. Skinner, Int. J. Inorg. Mater. 3 (2001) 113–121.
[15] N.D. Mathur, G. Burnell, S.P. Isaac, T.J. Jackson, B.S. Teo, J.L. MacManusDriscoll, L.F. Cohen, J.E. Evetts, M.G. Blamire, Nature 387 (1997) 266–268.
[16] F. Nolting, A. Scholl, J. Stohr, J.W. Seo, J. Fompeyrine, H. Siegwart, J.P. Locquet, S. Anders, J. Luning, E.E. Fullerton, M.F. Toney, M.R. Scheinfein, H.A. Padmore, Nature 405 (2000) 767–769.
[17] S. Iwanaga, M. Marciniak, R.B. Darling, F.S. Ohuchi, J. Appl. Phys. 101 (2007).
[18] S. Yamada, S. Nenno, Y. Matsumoto, N. Indayaningsih, J. Hombo, E. Sato, T. Shirakashi, S. Yoshihara, Denki Kagaku 62 (1994) 246–250.
[19] I. Hole, T. Tybell, J.K. Grepstad, I. Waernhus, T. Grande, K. Wiik, Solid State Electron. 47 (2003) 2279–2282.
[20] G.J. Snyder, R. Hiskes, S. DiCarolis, M.R. Beasley, T.H. Geballe, Phys. Rev. B 53 (1996) 14434–14444.
[21] W. Prellier, B. Mercey, J. Phys. D Appl. Phys. 35 (2002) L48–L51.
[22] L. Armelao, G. Bottaro, L. Crociani, R. Seraglia, E. Tondello, P. Zanella, Mater. Lett. 62 (2008) 1179–1182.
[23] L. Armelao, D. Barreca, G. Bottaro, A. Gasparotto, C. Maragno, Chem. Vapor Depos. 13 (2007) 112–117.
[24] L. Armelao, D. Barreca, G. Bottaro, A. Gasparotto, C. Maragno, E. Tondello, Chem. Mater. 17 (2005) 427–433.
[25] S. Schulz, S. Fahrenholz, D. Schuchmann, A. Kuczkowski, W. Assenmacher, F. Reilmann, N. Bahlawane, K. Kohse-Höinghaus, Surf. Coat. Technol. 201 (2007) 9071–9075.
[26] N. Bahlawane, P.A. Premkumar, J. Feldmann, K. Kohse-Hoinghaus, Chem. Vapor Depos. 13 (2007) 118–122.
[27] N. Bahlawane, P.A. Premkumar, K. Onwuka, G. Reiss, K. Kohse-Hoinghaus, Microelectron. Eng. 84 (2007) 2481–2485.
[28] N. Bahlawane, S. Blittersdorf, K. Kohse-Hoinghaus, B. Atakan, J. Muller, J. Electrochem. Soc. 151 (2004) C182–C186.
[29] A.J. Zhou, T.J. Zhu, X.B. Zhao, Mater. Sci. Eng. B Solid State Mater. Adv. Technol. 128 (2006) 174–178.
[30] R. Koc, H.U. Anderson, J. Mater. Sci. 27 (1992) 5837–5843.
[31] R. Koc, H.U. Anderson, J. Eur. Ceram. Soc. 15 (1995) 867–874.
[32] S.R. Sehlin, H.U. Anderson, D.M. Sparlin, Solid State Ion. 78 (1995) 235–243.
[33] M.H. Hung, M.V.M. Rao, D.S. Tsai, Mater. Chem. Phys. 101 (2007) 297–302.
[34] N. Fujihira, T. Sei, T. Tsuchiya, J. Sol–Gel Sci. Technol. 4 (1995) 135–140.
[35] M. Losurdo, A. Sacchetti, P. Capezzuto, G. Bruno, L. Armelao, D. Barreca, G. Bottaro, A. Gasparotto, C. Maragno, E. Tondello, Appl. Phys. Lett. 87 (2005).
[36] K. Gaur, S.C. Verma, H.B. Lal, J. Mater. Sci. 23 (1988) 1725–1728.
[37] R. Robert, L. Bocher, M. Trottmann, A. Reller, A. Weidenkaff, J. Solid State Chem. 179 (2006) 3893–3899.
[38] R. Raffaelle, H.U. Anderson, D.M. Sparlin, P.E. Parris, Phys. Rev. B 43 (1991) 7991–7999.
[39] L.W. Tai, M.M. Nasrallah, H.U. Anderson, D.M. Sparlin, S.R. Sehlin, Solid State Ion. 76 (1995) 259–271.
[40] M.A. Senarisrodriguez, J.B. Goodenough, J. Solid State Chem. 116 (1995) 224–231.
[41] I. Solovyev, N. Hamada, K. Terakura, Phys. Rev. B 53 (1996) 7158–7170.
[42] D.D. Sarma, N. Shanthi, S.R. Barman, N. Hamada, H. Sawada, K. Terakura, Phys. Rev. Lett. 75 (1995) 1126–1129.
[43] P. Gerthsen, K.H. Hardtl, Zeit. Nat. Part A Astrophys. Phys. Phys. Chem. A 17 (1962) 514.
[44] P. Dordor, S. Joiret, J.P. Doumerc, J.C. Launay, J. Claverie, P. Hagenmuller, Phys. Status Solidi A Appl. Res. 93 (1986) 321–328.
[45] G.H. Jonker, Philips Res. Rep. 24 (1969) 1.
[46] V.G. Bhide, D.S. Rajoria, C.N.R. Rao, G.R. Rao, V.G. Jadhao, Phys. Rev. B 12 (1975) 2832–2843.
[47] R. Mahendiran, A.K. Raychaudhuri, A. Chainani, D.D. Sarma, S.B. Roy, Appl. Phys. Lett. 66 (1995) 233–235.
[48] T. Arima, Y. Tokura, J.B. Torrance, Phys. Rev. B 48 (1993) 17006–17009.
[49] A. Chainani, M. Mathew, D.D. Sarma, Phys. Rev. B 46 (1992) 9976–9983.
[50] T. Saitoh, A.E. Bocquet, T. Mizokawa, H. Namatame, A. Fujimori, M. Abbate, Y. Takeda, M. Takano, Phys. Rev. B 51 (1995) 13942–13951.
[51] D.P. Karim, A.T. Aldred, Phys. Rev. B 20 (1979) 2255–2263.
[52] M.V. Patrakeev, J.A. Bahteeva, E.B. Mitberg, I.A. Leonidova, V.L. Kozhevnikov, K.R. Poeppelmeier, J. Solid State Chem. 172 (2003) 219–231.